Ai, Q., Kamliya Jawahar, H., & Azarpeyvand, M. (2016). Experimental Investigation of Aerodynamic Performance of Airfoils Fitted with Morphing Trailing Edges. In *54th AIAA Aerospace Sciences Meeting* [AIAA 2016-1563] American Institute of Aeronautics and Astronautics Inc. (AIAA). https://doi.org/10.2514/6.2016-1563

Experimental investigation of aerodynamic performance of airfoils fitted with morphing trailing edges

Qing Ai*, Hasan Kamliya Jawahar† and Mahdi Azarpeyvand‡
University of Bristol, Bristol, United Kingdom, BS8 1TR

The aerodynamic performance and wake development of a NACA 0012 airfoil fitted with morphing trailing edges were studied using experimental and computational techniques. The NACA 0012 airfoil was tested with morphing trailing edges having various camber profiles with the same trailing edge tip deflection. The aerodynamic force measurements for the airfoil were carried out for a wide range of chord-based Reynolds number and angles of attack with trailing edge deflection angle of $\beta = 5°$ and $10°$. The experiments were validated with steady-state RANS simulation using Spalart-Allmaras turbulence model. Experimental results show that the camber profiles of the morphing trailing edges significantly affect the airfoil's aerodynamic performance and effectiveness in improving the lift coefficient further by tailoring the morphing profiles. Hot-wire measurements showed that the downstream wake development can also be influenced as a result of changing the morphing trailing edge camber profile. It was found that highly cambered trailing edge profiles provide higher lift coefficients and increased maximum lift coefficient compared to moderately cambered profiles while the lift-to-drag ratio slightly decreases. Velocity contour plots show that the separation near the trailing edge is further delayed at high angles of attack for airfoils with highly chambered morphing trailing edge. This study shows that the effective design space of the morphing trailing edges can be expanded taking into account the optimal aerodynamic performance requirements. The study also suggests that in order to achieve optimum aerodynamic performance, independent surface morphing of the suction and pressure surface camber will be required to delay the onset of flow separation.

Nomenclature

b	=	trailing edge chord length
c	=	airfoil chord length
C_L	=	lift coefficient
$C_{L,max}$	=	maximum lift coefficient
C_D	=	drag coefficient
D	=	drag force
l	=	airfoil span length
L	=	lift force
Re_c	=	chord-based Reynolds number
S	=	wing area, m^2
U	=	free stream velocity, m/s
α	=	angle of attack, °
β	=	morphing trailing edge tip deflection angle, °
ρ	=	air density, kg/m^3
y^+	=	dimensionless wall distance

*PhD Student, Advanced Composites Centre for Science and Innovation (ACCIS), University of Bristol. Qing.ai@bristol.ac.uk

†PhD Student, Department of Aerospace Engineering, AIAA Student Member, hasan.kj@bristol.ac.uk

‡Senior Lecturer and Royal Academy of Engineering Research Fellow, Department of Mechanical Engineering, m.azarpeyvand@bristol.ac.uk

I. Introduction

Aviation has grown rapidly over the past decades and attention has been attracted to the adverse environmental impact including the noise and green gas emissions. Future expansion of aviation puts more pressure on the aerospace industries to address these issues. In the Flightpath 2050 goals of protecting environment and the energy supply by Advisory Council for Aviation Research and Innovation in Europe [1], the CO_2 emissions per passenger kilometre is expected to be reduced by 75%, NO_x emissions by 90% and perceived noise by 65%. Technological efforts and improvements are necessary to meet the emission reduction goals, including utilization of light-weight materials, new aircraft configurations, innovative propulsion system design and novel high-lift systems. One particular topic is the morphing structure, which is considered as a promising candidate for the next generation of aircraft high-lift systems [2].

The shape change of aircraft wing through control surfaces including leading edge slats and trailing edge flaps has been widely used for lift and drag control during take-off and landing. These conventional mechanical high-lift systems increase the wing design complexity and also are considered as significant noise sources due to the presence of hinge fairings and flap edges cavities. Morphing structures that are light-weight and remain conformal to the wing have been studied due to their potential to improve the high-lift system performance. Unlike mechanical control devices, the proposed morphing technologies adapts to the variational flow conditions through structural deformation instead of rigid body movements, leading to conformal systems and smooth structural surfaces [3]. Research activities regarding morphing concepts development, demonstrator testing and modelling and optimization design have been carried out and several reviews of relevant morphing concepts are available, see Refs. [4–8], for applications of morphing structures in the aerospace, automotive and wind turbine industries.

Studies have shown that the deformation shape and curvature of the morphing structure significantly affects the aerodynamic performance of the airfoils [9–16]. Sanders *et al.* [9] conducted investigations on airfoils fitted with conventional flaps and conformal morphing trailing edges. It was found that the conformal morphing trailing edge has some distinct aerodynamic benefits over conventional mechanical flaps and the pressure distribution over the airfoil was found to be dependent on the shape of the deformed control surfaces. Daynes *et al.* [10] showed that a morphing flap can provide the same change in lift coefficient with a 30% less tip deflection compared to a hinged flap of equal flap length. This enhanced control effectiveness is believed to originate from the differing geometries. Wolff *et al.* [12] conducted a two-dimensional numerical investigation of a wind turbine airfoil fitted with morphing trailing edges and found that the deformed morphing trailing edge significantly affects the lift coefficient and stall behaviour of the airfoil. Results showed that the changes to the lift coefficient are dependent on the size, curvature and deflection angle of the deformed trailing edge and strongly curved deformed trailing edge can produce lower maximum lift-to-drag ratio and also increased the root bending moment coefficient compared to a gently curved deformed trailing edge. Campanile *et al.* [13] developed a belt-rib morphing airfoil concept and proposed a model to study the possible actuation requirement reduction by exploiting the aerodynamic and aeroelastic amplification effects on airfoils. Effects of different deformation modes of morphing airfoil and conventional airfoil using hinged flap were quantitatively evaluated and results show that higher slope at trailing edge of belt-rib airfoil leads to large change in lift. In a more recent study, Ai *et al.* [14, 15] proposed a novel morphing trailing edge design using honeycomb core of axial variable stiffness and proved that introducing variable stiffness materials into the morphing structures could change the actuation energy of the system and also enable the tailoring of the morphing profiles, which significantly affects the aerodynamic and aeroacoustic performance of the airfoils. Yokozeki *et al.* [16] developed a morphing airfoil concept using corrugated structures and wind tunnel tests of the demonstrator showed that the morphing wing presented superior properties in lift coefficient compared to a reference wing using conventional flap, which was believed to result from the seamless morphing deformation.

In this paper, experimental and numerical studies are conducted to investigate the effects of morphing profiles on the aerodynamic and aeroacoustic performance of airfoils. A NACA0012 airfoil is chosen for the tests and fitted with a series of morphing trailing edges which have a same tip deflection but with different camber profiles. Wind tunnel tests including aerodynamic forces measurements, wake development analysis are carried out on a wing model. Computational fluid dynamic (CFD) simulations are also carried out using OpenFoam, which validates the experimental results and studies the aerodynamic performance of the airfoils.

II. Experimental and Computational Setup

A. Experimental Setup and Measurement Techniques

Aerodynamic force measurements and wake development of a NACA 0012 airfoil fitted with morphing trailing edges having various camber profiles have been experimentally tested at the University of Bristol wind tunnel facilities; (i) low speed closed-circuit wind tunnel that has an octagonal working area of 2.1 m × 1.5 m × 2 m, with a contraction ratio of 3:1 and a stable working velocity range of 10 m/s to 60 m/s and (ii) open jet wind tunnel with diameter of 1.1 m, with a maximum reliable speed of 30 m/s and minimum turbulence level of 0.05%.

1. Force Measurement Setup

Force measurements were carried out in the large low speed closed circuit wind-tunnel. The blockage effects were found to be negligible. In order to mitigate the flow three dimensionality effects around the airfoil model in the tunnel, two circular end-plates with a radius of 0.17 m were attached to the airfoil, as shown in Fig. 1a. The aerodynamic force measurements of the lift (L) and drag (D) forces were measured using an AMTI OR6-7-2000 force platform (Serial No.5501) from Advanced Mechanical Technology Inc., mounted at the base of the set-up. The force platform records the force-induced voltage measured through AMTI MSA-6 strain gauge amplifiers and signal data were collected using LabView V18 software. Digital signals of six channels ($F_x, F_y, F_z, M_{xy}, M_{xz}, M_{yz}$) are monitored and transformed to force data using a sensitivity matrix provided by the Advanced Mechanical Technology Inc. The data sampling frequency and sampling period were selected to be 37 Hz and 30 s after a thorough uncertainty analysis of the results.

2. Wake Measurements Setup

Steady and unsteady flow velocities at different streamwise locations within the airfoil wake were measured using a Dantec 55P16 single hot-wire probe with a 5 μm diameter and 1.25 mm long platinum-plated tungsten wire sensor. The temperature probe was connected to StreamWare Pro V5.14 software package, driven by Dantec Streamline Pro CTA 91C10 modules and controlled using National Instrument NI9215 four channel module. Calibrations were conducted for the probe using a Dantec 54H10 two point mode hot-wire calibrator. The data logging frequency was set to be 40 kHz and time duration was 20 s. The probe was mounted on a 1 m long slender cylindrical steel arm connected to the traverse system to minimise the effect of the traverse system on the airfoil and wind tunnel. The closest point measured to the airfoil was at 2 mm for the tested angles of attack.

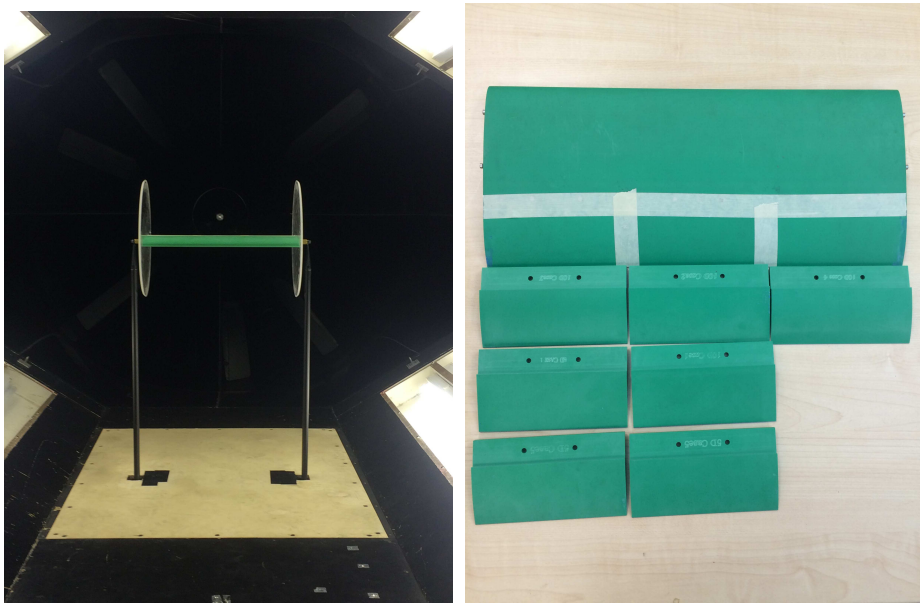

a) Wing set-up in tunnel **b) Wing and trailing edges**

Figure 1. Wind tunnel setup and airfoil geometry with the interchangeable trailing edges.

B. Morphing Trailing-edge Setup

NACA 0012 airfoil model (Fig. 1b) with a chord length of $c = 0.2$ m and a span of $l = 0.45$ m was manufactured using RAKU-TOOL WB-1222 polyurethane board and machined using a computer aided numerically controlled machine. The airfoil was designed to facilitate multiple interchangeable trailing edges of 30% chord length (60 mm) with the required camber profile and deflection angle. The aerodynamic and aeroacoustic performance of novel morphing trailing edge Ai *et al.* [14, 15] were tested using Xfoil-BPM model and as a further continuation this study five morphing trailing edges having camber profiles from plain flap to highly cambered conformal morphing trailing edges (see Fig. 2) were developed for this current detailed experimental study. Morphing trailing edge deflection angle is defined using the ratio between the flap length, b and tip deflection, with positive deflection angles in the direction of the pressure side, as shown in Fig. 2. The airfoils were tested for morphing trailing edges with varying camber profiles for deflection angles, $\beta = 10°$ (Case 1 to Case 5) and $\beta = 5°$ (Case 1 to Case 3). The first cases of both tip angles represents a typical hinged flap movement and the following cases employ an increasingly cambered conformal morphing trailing edge profiles.

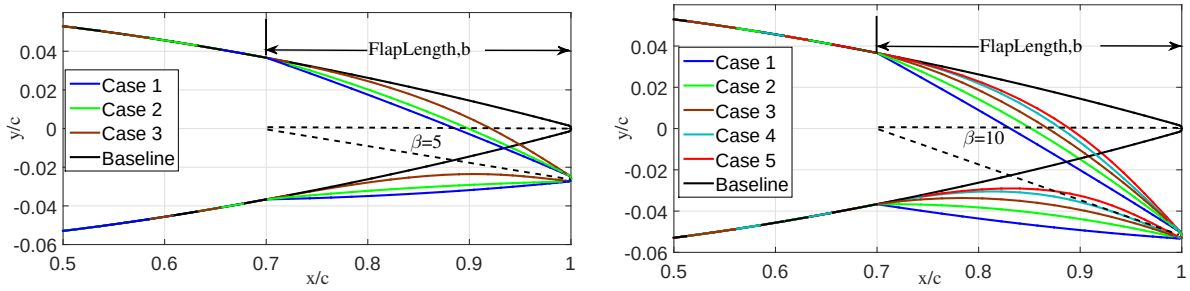

a) deflection angle of β=5° **b) deflection angle of β=10°**

Figure 2. NACA 0012 airfoil fitted with different morphing trailing edges.

C. Computational Setup

Steady state computational studies have been carried out to validate the experiments and further investigate the effects of morphing profiles on flow behaviour around the airfoil and its wake development. Reynolds-averaged Navier-Stokes (RANS) numerical simulations were performed using OpenFOAM open source code and Spallart-Allmaras (S-A) turbulence Model. The computational domain and the two dimensional grid was created using commercial software ICEM-CFD (see Fig. 3). After a domain independence study the domain size was set to be $10c$ on the crosswise and $20c$ on the streamwise direction. A C-grid topology with hexahedral structured grid were employed for the current study. Grid independence study with elements ranging from 50,000 to 500,000 were carried out and a domain with 285,000 grid elements with highly dense wake grid was selected for the simulations presented here. In order to accurately capture the boundary layer the airfoil wall was set to have a y^+ value of 0.5-1. To capture the flow separation accurately close to the wall, the first 7 mm from the airfoil was densely populated with 50 grid points. To capture the wake accurately the the first $1.5c$ just aft of the airfoil was densely populated with 300 grid points.

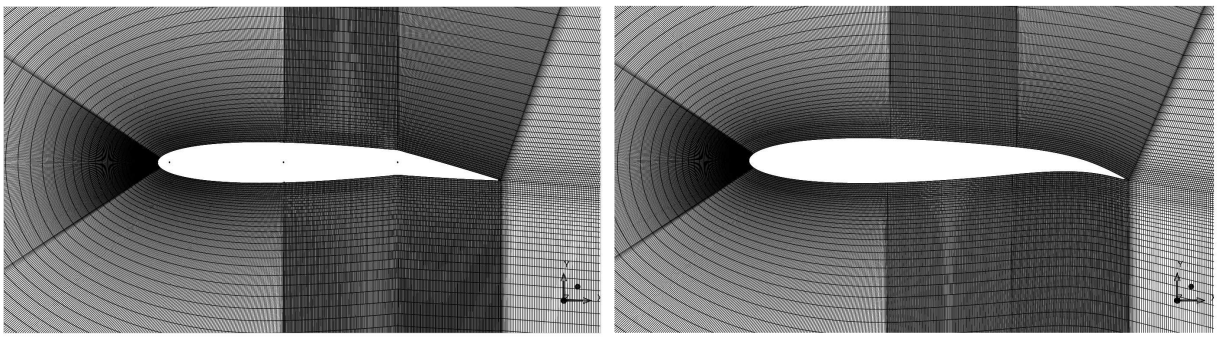

a) Case 1 **b) Case 5**

Figure 3. NACA 0012 morphed trailing edge with flap deflection angle of $\beta = 10°$.

III. Results and Discussion

A. Aerodynamic Forces Measurements

The aerodynamic force (lift and drag) measurements of a NACA 0012 airfoil with chord $c = 0.2$ m fitted with morphing trailing edges were carried out for a wide range of flow velocities $U = 25$ m/s, 32 m/s and 40 m/s, corresponding to chord-based Reynolds number of $Re_c = 3.5 \times 10^5$, 4.5×10^5 and 5.6×10^5, respectively. The airfoil was tested with interchangeable morphing trailing edges with deflection angles, $\beta = 5°$ and $10°$ and for a wide range of angles of attack, $\alpha = -5°$ to $20°$. The morphing trailing edge with deflection angle $\beta = 5°$ was tested for three trailing edge camber profiles (Case 1 to Case 3) and $\beta = 10°$ for five trailing edge camber profiles (Case 1 to Case 5).

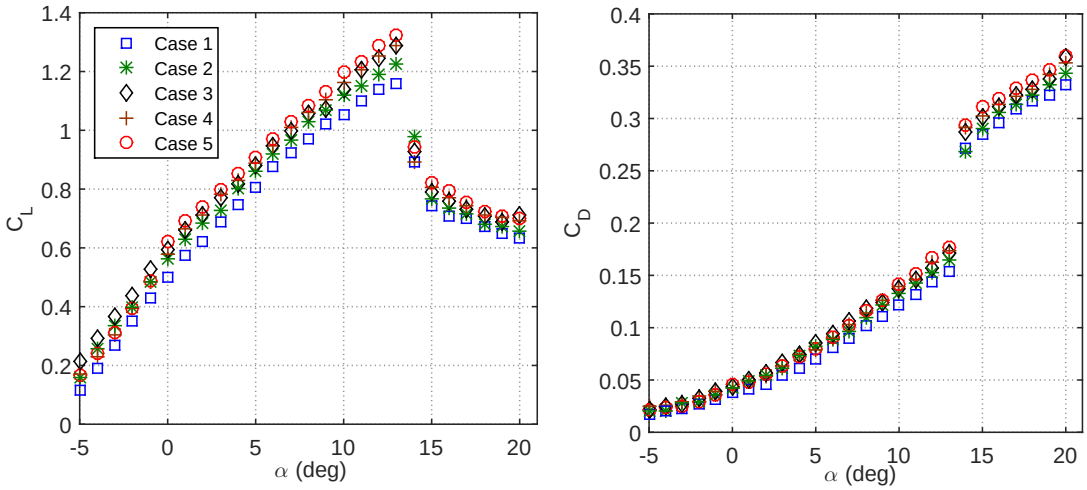

Figure 4. Lift and drag coefficient results for NACA 0012 airfoil fitted with various morphing trailing edges of $\beta = 10°$, at the flow velocity of $U = 25$ m/s ($Re_c = 3.5 \times 10^5$).

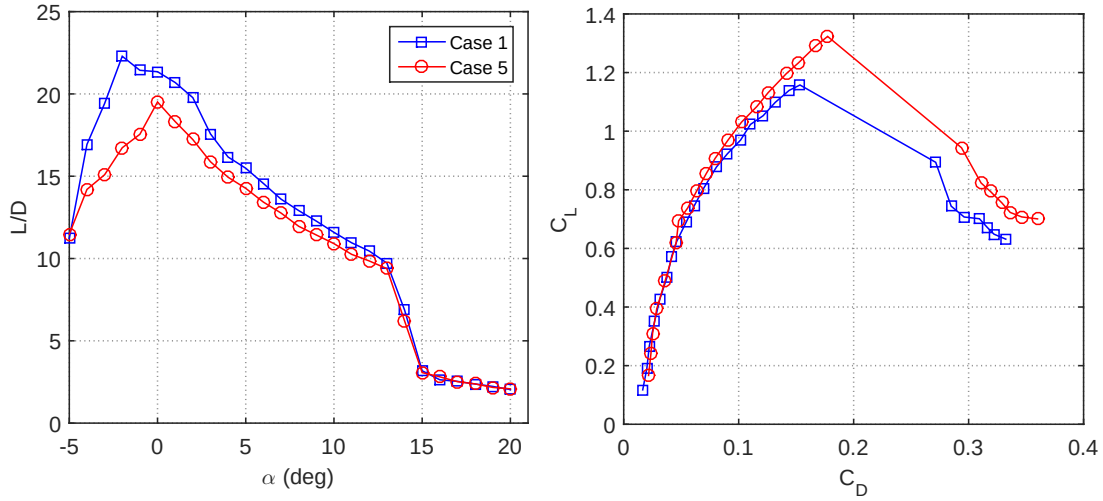

Figure 5. The lift-to-drag ratio (left) and polar plot of $C_L - C_D$ (right) of a NACA 0012 airfoil fitted with morphing trailing edge of $\beta = 10°$, at the flow velocity of $U = 25$ m/s ($Re_c = 3.5 \times 10^5$).

Figure 4 presents the lift (C_L) and drag coefficient (C_D) for NACA 0012 airfoil with trailing edge deflection angle of $\beta = 10°$ for all the five different trailing edge camber profiles, tested at flow velocity of $U = 25$ m/s, corresponding to $Re_c = 3.5 \times 10^5$. The C_L and C_D results clearly show that the variation in the morphing trailing edge camber profiles significantly affects the C_L and C_D for the tested angles of attack range. The results show an increase in $C_{L,max}$ of up to 13% in the case of highly cambered profile (Case 5) compared to the hinged flap profile (Case 1) just before entering stall at $\alpha = 13°$. The C_L for Case 1 with the hinged flap has the lowest $C_L - \alpha$ curve out of all the tested camber profiles. This will be further discussed in the following section. Case 5 with the highly cambered morphing trailing

edge profile has the highest C_L for angles of attack ranging from $\alpha = 0°$ to 20°. Case 5 at lower angles of attack, $\alpha = -5°$ to 0° appears to have reduced performance close to that of Case 2. Case 3 has the best performance with the highest C_L at negative and lower angles of attack from $\alpha = -5°$ to 0°. Figure 4 also shows that at stall angle of attack, $\alpha = 13°$, the C_D of Case 5 is up to 14% greater than that of the Case 1. The overall C_D performance of the morphing trailing edge cases increases with the increase in trailing edge camber profile. Case 5 having the highest morphing trailing edge camber has the highest C_D amongst all the other cases.

Figure 5 shows the lift-to-drag (L/D) ratio results of Case 1 and Case 5. It is evident from these results that the overall L/D ratio of Case 1 is larger than that of Case 5. At negative angles of attack, $\alpha = -2°$ it can be observed that Case 1's L/D is about 25% greater than that of Case 5, however this large difference gradually decreases as the angles of attack increase. The L/D difference between the cases decreases to 9% at $\alpha = 0°$, 8% at $\alpha = 10°$ and to just 4% at stall angle of attack $\alpha = 13°$. The polar curves of C_L and C_D in Fig. 5 summarises the lift and drag performance between Case 1 and Case 5, showing that Case 5 has increased C_L and C_D as the angles of attack increases, especially close to stall angle. Note, however, that the stall angle of attack is not found to change as a result of morphing trailing edge profiles and further studies are necessary for understanding the post-stall properties and flow behaviour. Even though the aerodynamic force measurements were carried out for three different velocities only $U = 25$ m/s was presented here as the C_L and C_D were found to be independent of Reynolds number for the flow velocities tested here. The cases with trailing edge deflection angle $\beta = 5°$ are not presented here as the difference between the three tested cases were insignificant for in depth discussion. Results, however suggest that the effect of morphing profile will be ever more important for larger deflection angles (β), which requires more investigation.

B. Wake Development

Detailed flow field measurements at downstream wake locations were performed using hot-wire anemometry to further understand the flow behaviour due to the cambered profile at the trailing edge. The wake measurements were carried out for NACA 0012 airfoil fitted with morphing trailing edge with deflection angle $\beta = 10°$. Only two trailing edge camber profiles (Case 1 and Case 5) with the best and worst aerodynamic performance were selected for the wake development study. The tests were performed in the large Open-jet wind tunnel for angles of attack, $\alpha = 0°$, 2°, 4° and 6° at flow velocity $U = 20$ m/s, corresponding to $Re_c = 2.6 \times 10^5$.

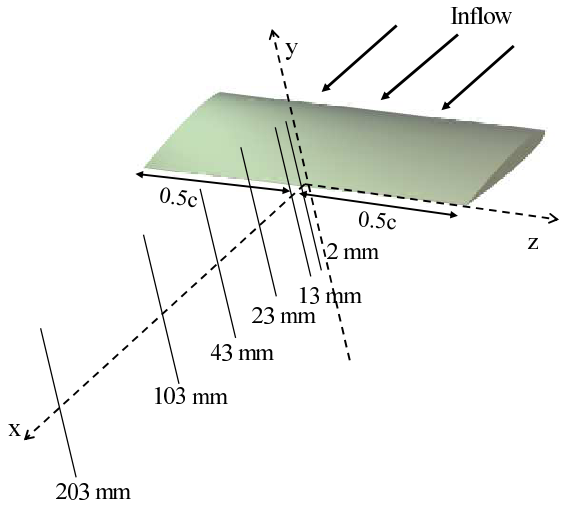

Figure 6. Chord-wise locations of flow velocity measurements in hot-wire anemometry.

The wake measurements were made at six downstream locations in the mid-span position of the airfoil in the streamwise direction, $x = 2$ mm, 13 mm, 23 mm, 43 mm, 103 mm and 203 mm with the trailing edge tip assumed as the datum point (x and $y = 0$) as shown in Fig. 6. Each measurement line was densely populated with several data sampling positions according to the wake profile peak locations predicted from preliminary CFD simulations. Even though measurements were made for four different angles of attack but only two angles of attack, $\alpha = 0°$ and 4° are presented and discussed here for the purpose of brevity. The experimental results presented here are validated with its corresponding CFD results whenever possible.

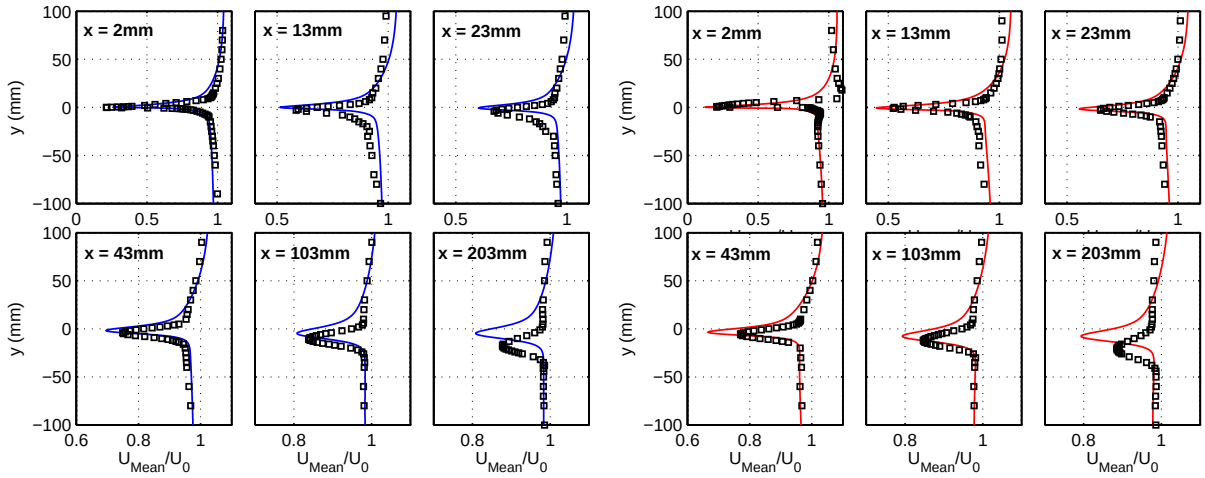

a) CFD Case 1 —, Exp Case 1 □ b) CFD Case 5 —, Exp Case 5 □

Figure 7. Wake development of Case1 and Case 5 at angle of attack, $\alpha = 0°$ for flow velocity $U = 20$ m/s ($Re_c = 2.6 \times 10^5$).

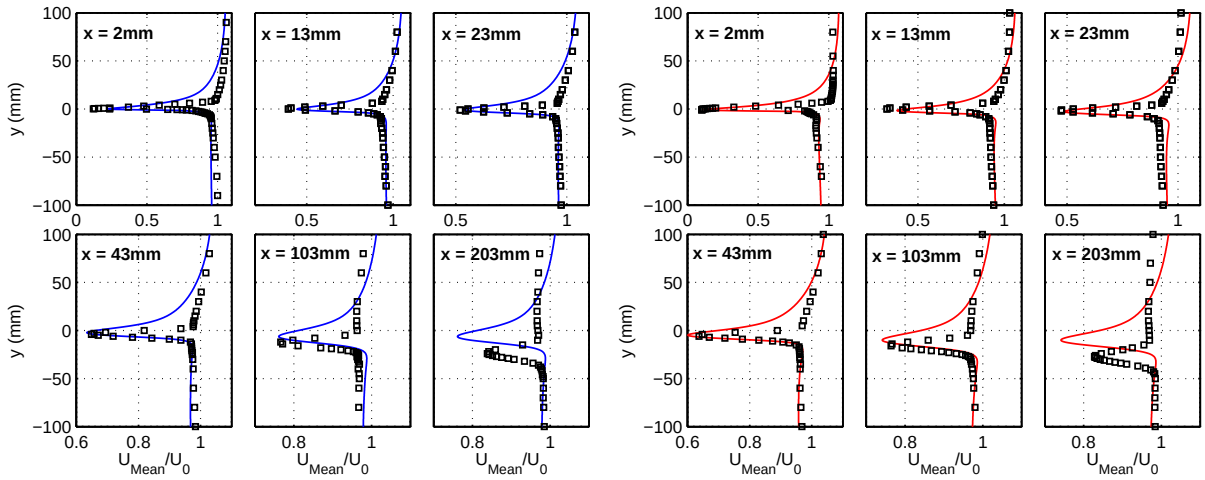

a) CFD Case 1 —, Exp Case 1 □ b) CFD Case 5 —, Exp Case 5 □

Figure 8. Wake development of Case1 and Case 5 at angle of attack, $\alpha = 4°$ for flow velocity $U = 20$ m/s ($Re_c = 2.6 \times 10^5$).

The normalised wake velocity profiles for NACA 0012 airfoil with morphing trailing edge with deflection angle $\beta = 10°$ and angle of attack $\alpha = 0°$ are shown in Fig. 7 for flow velocity of $U = 20$ m/s, corresponding to $Re_c = 2.6 \times 10^5$. It can be observed that the S-A turbulence model accurately predicts the velocity deficit and peak location compared to that of the experimental data at the near-wake locations, namely $x = 2$ mm, 13 mm and 23 mm. At far-wake locations, $x = 43$ mm and 103 mm, the S-A model predicts the velocity deficit for Case 1 in Fig. 7a quite accurately but overpredicts the velocity deficit for Case 5 in Fig. 7b. The S-A model predicts the wake width to be larger than the experimental results for both Case 1 and Case 5 at far-wake location $x = 103$ mm. At far-wake location, $x = 203$ mm S-A model fails to predict the velocity deficit, wake width and the peak location. The peak location of the experimental data sets for both the Case 1 and Case 5 have a larger flow deflection angle (flow turning angle) compared to the S-A model prediction. The S-A model's failure to accurately predict the flow at far-wake locations are mostly due to not incorporating the open-jet wind tunnels effects into the simulation. It is noteworthy, that Case 5 has a larger wake deflection at the far-wake locations at $x = 103$ mm and 203 mm, which adds to the lift produced from the downwash. This also corresponds to the higher C_L of the Case 5 seen in the previous section.

Figure 8 shows the normalised wake velocity profiles for Case 1 and Case 5 for angle of attack $\alpha = 4°$. The S-A model has accurately predicted the peak location and velocity deficit at near-wake locations at $x = 2$ mm, 13 mm and 23 mm, however the wake profile of the suction side appears to have separated flow while the experimental results do not show such behaviour. At far-wake locations, $x = 43$ mm and 103 mm, the S-A model predicts the velocity deficit for the Case 1 and Case 5 quite accurately but overpredicts the velocity deficit for far-wake location $x = 203$ mm. The S-A model predicts wake width to be larger than the experiments for both the Case 1 and Case 5 for all the downstream far-wake locations, $x = 43$ mm, 103 mm and 203 mm. The increased flow deflection angle for Case 5 compared to Case 1 results can also be observed from the peak locations at $x = 103$ mm and 203 mm.

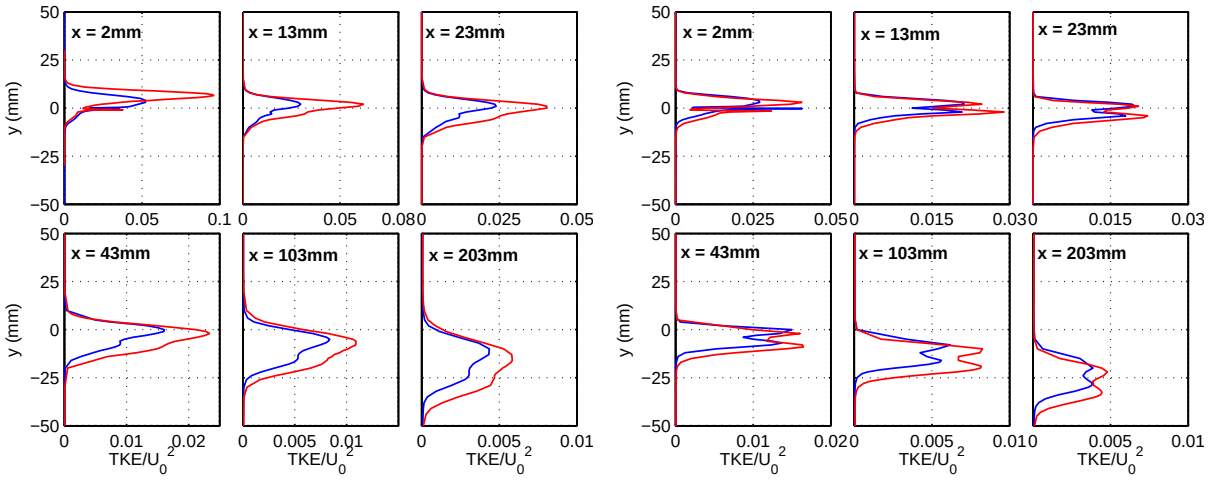

a) $\alpha = 0°$ **b)** $\alpha = 4°$

Figure 9. Turubulent Kinetic Energy within the wake region for Case 1 — and Case 5 —.

The turbulent kinetic energy (TKE) profiles from the experimental measurements for NACA 0012 airfoil with morphing trailing edge having camber profiles Case 1 and Case 5 for angles of attack $\alpha = 0°$ and $\alpha = 4°$ are shown in Figs. 9a and 9b, respectively. For angle of attack $\alpha = 0°$, at near-wake location, $x = 2$ mm close to the trailing edge, it can be observed that the TKE magnitude for Case 5 is about 50% higher than Case 1 and at $x = 13$ mm it is 60% higher than Case 1. This difference in TKE magnitude between the cases reduces at further downstream locations. At far-wake locations, $x = 43$ mm, 103 mm and 203 mm, it can be observed that Case 5 has a much wider wake towards the pressure surface than that of Case 1. From the peak location of the TKE profiles at far-wake locations, $x = 43$ mm, 103 mm and 203 mm, aforementioned increased deflection angle of Case 5 can be observed readily. The TKE profiles at angle of attack, $\alpha = 4°$ for both morphing cases are shown in Fig. 9b. From the results it can be observed that the TKE magnitude has a dual peak nature, which was absent at lower angle of attack $\alpha = 0°$ the large difference in TKE magnitude seen between Case 1 and Case 5 at lower angle of attack $\alpha = 0°$ is not observed here, however there is still a noticeable difference in TKE magnitude between the cases, with Case 5 having larger TKE magnitude. The increased deflection of the wake for Case 5 compared to Case 1 can also be readily observed for $\alpha = 4°$ at far-wake locations, $x = 43$ mm, 103 mm and 203 mm.

The mean velocity contours for NACA 0012 airfoil with morphing trailing edge for angles of attack $\alpha = 0°$ and $\alpha = 4°$ with trailing edge deflection angle $\beta = 10°$ are shown in Figs. 10 and 11 respectively. From the mean velocity contour plots for angle of attack $\alpha = 0°$ in Fig. 10 it can be observed that for Case 1 the separation on the suction side occurs at around $0.8c$, whereas for Case 5 the separation is delayed by the smooth cambered profile and it occurs at around $0.9c$. For Case 1 the separation on the pressure side occurs just before the hinge of the flap at $0.6c$ and reattaches to the surface at around $0.7c$ before mixing into the airfoil wake. For Case 5 the separation on the pressure side occurs at around $0.6c$ and only reattaches at $1c$ close to the tip of the trailing edge just before separating and mixing into the airfoil wake. This large separation with possible small scale recirculation between locations $0.6c$ and $1c$ on the pressure side for Case 5 could be the primary reason for the larger wake velocity deficit compared to Case 1 as discussed in previous sections. This separation on the pressure side for Case 5 also appears to have an influence on the velocity reduction in the nearby surrounding area, which corresponds to the wider wake discussed earlier in the previous section.

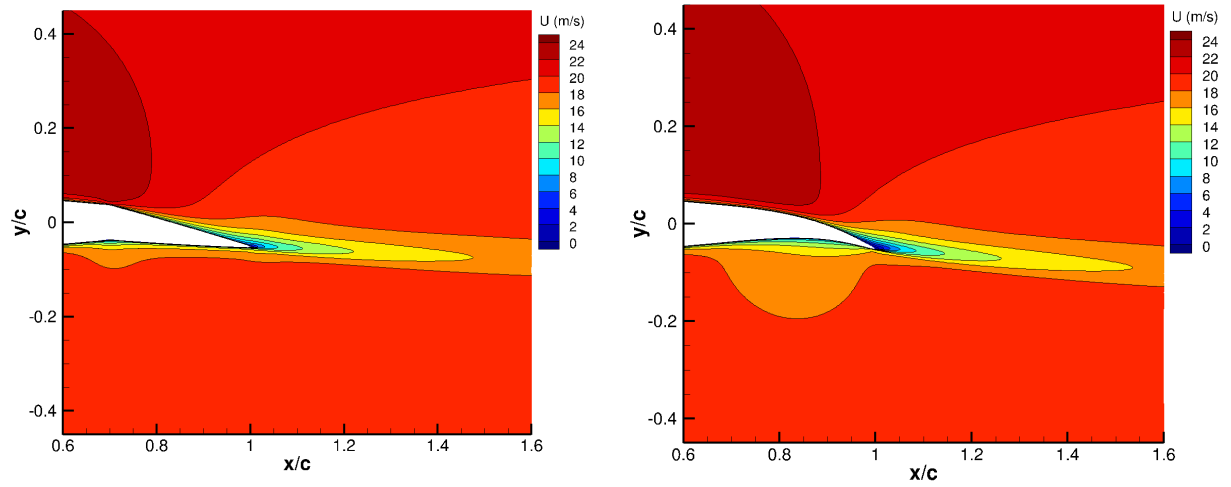

a) Case 1 b) Case 5

Figure 10. NACA 0012 morphed trailing edge cases with angle of attack, $\alpha = 0°$ and flap deflection angle of $\beta = 10°$ for flow velocity of $U = 20$ m/s ($Re_c = 2.6 \times 10^5$).

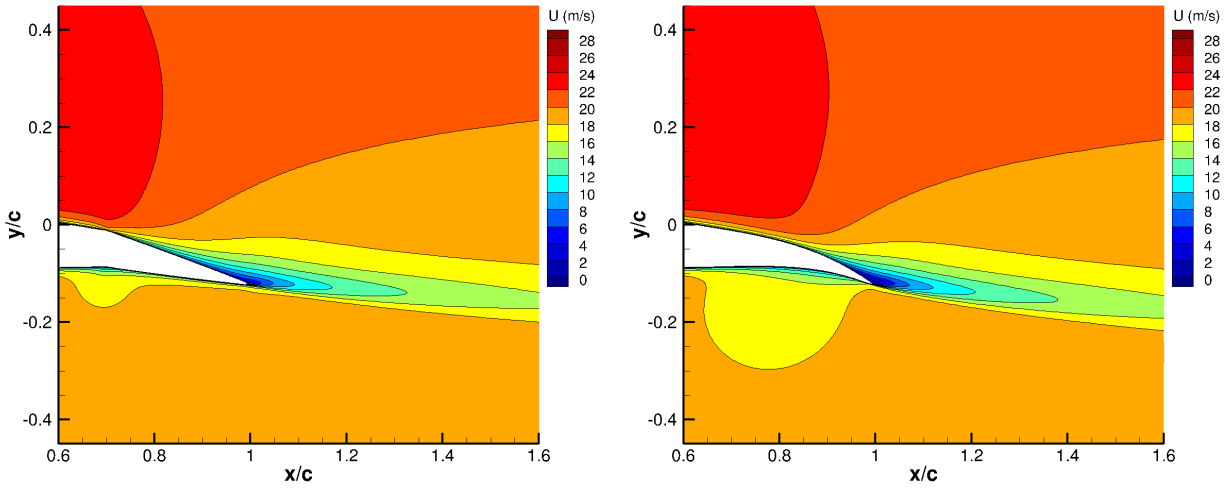

a) Case 1 b) Case 5

Figure 11. NACA 0012 morphed trailing edge cases with angle of attack, $\alpha = 4°$ and flap deflection angle of $\beta = 10°$ for flow velocity of $U = 20$ m/s ($Re_c = 2.6 \times 10^5$).

From the mean velocity contour plots for angle of attack $\alpha = 4°$ in Fig. 11 it can be observed that for Case 1 the separation on the suction side occurs slightly earlier than seen at lower angle of attack $\alpha = 0°$, where the separation on the suction side occurs at $0.7c$, at the flap hinge point. However, for Case 5 the separation on the suction side is much delayed and occurs at around $0.85c$, close to the separation location observed at lower angle of attack $\alpha = 0°$. For angle of attack $\alpha = 4°$ the flow separation on the pressure side for Case 1 is the same as that of $\alpha = 0°$, where the separation occurs just before the hinge of the flap at $0.6c$ and reattaches to the surface at around $0.7c$ before mixing into the airfoil wake. For Case 5 at angle of attack $\alpha = 4°$ the separation on the pressure side occurs at around $0.7c$ and only reattaches at $1c$, at the tip of the trailing edge just before separating and mixing into the airfoil wake. The onset of this large separation on the pressure side of Case 5 appears to be further delayed with increase in angle of attack. The separation for Case 5 on the pressure side always appears to be larger than that of Case 1 resulting in increased wake velocity deficit that adds to the increased form drag for Case 5 as observed in previous section. This large flow separation on the pressure side of the highly cambered trailing edge profiles can be avoided by the use of independent surface morphing, since the cambered trailing edge results in favourable delayed separation on the suction side but also results in unfavourable early separation on the pressure side. An optimum design would require a different camber

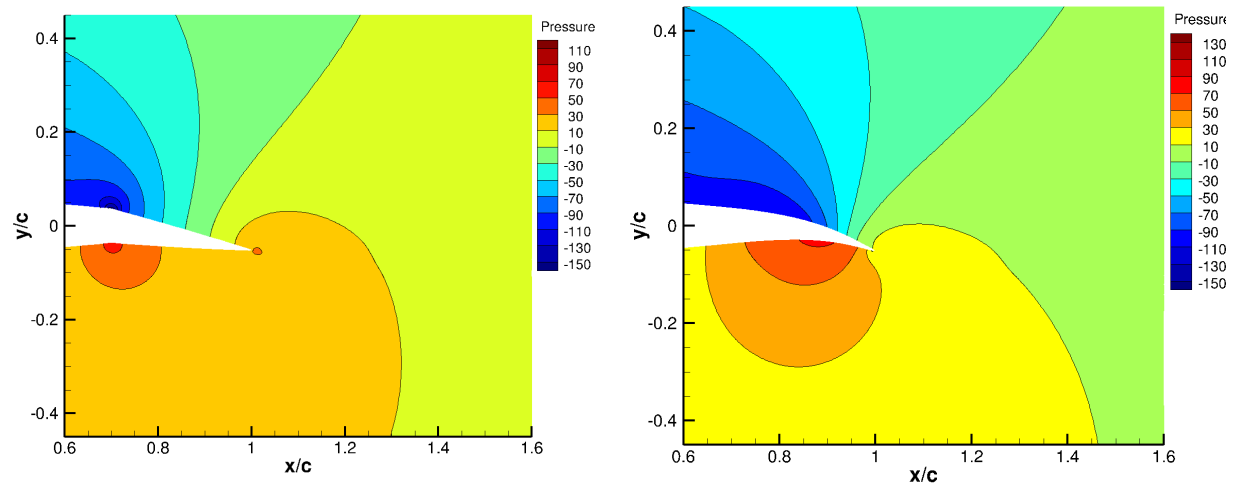

a) Case 1 b) Case 5

Figure 12. NACA 0012 morphed trailing edge cases with angle of attack, $\alpha = 0°$ and flap deflection angle of $\beta = 10°$ for flow velocity of $U = 20$ m/s ($Re_c = 2.6 \times 10^5$).

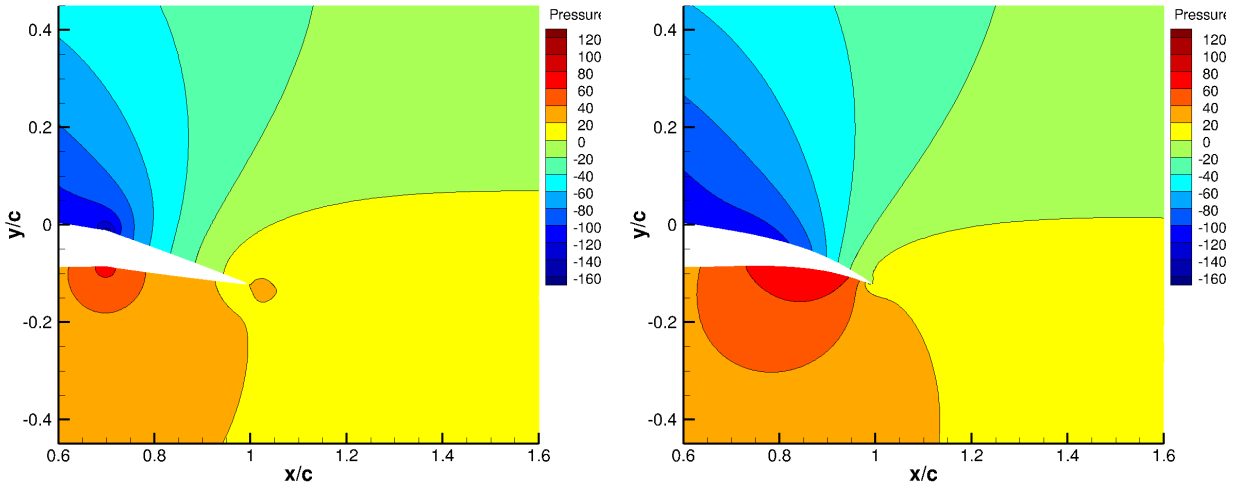

a) Case 1 b) Case 5

Figure 13. NACA 0012 morphed trailing edge cases with angle of attack, $\alpha = 4°$ and flap deflection angle of $\beta = 10°$ for flow velocity of $U = 20$ m/s ($Re_c = 2.6 \times 10^5$).

profile for the pressure side to delay the onset of early separation on the lower side of the trailing edge.

The pressure distribution contours for NACA 0012 airfoil with morphing trailing edge for angles of attack $\alpha = 0°$ and $\alpha = 4°$ with trailing edge deflection angle $\beta = 10°$ are shown in Figs. 12 and 13, respectively. The results from Figs. 12 and 13 show that the pressure drop on the suction side of the airfoil is evenly distributed up till $0.9c$ for Case 5, whereas for Case 1 the pressure drop on the suction side closer to the trailing edge is dispersedly distributed. The results clearly show the location of flow separation on both the suction and pressure sides for both Case 1 and Case 5 and angles of attack $\alpha = 0°$ and $4°$. The pressure increase on the pressure side of the morphing trailing edge can be observed for both Case 1 and Case 5, the high pressure area is contained within the radius of the hinge for Case 1, but it is spread over the entire flap for Case 5. This high pressure is due to the reduced velocity from the separation on the pressure side and it might be also due to possible small scale flow recirculation.

The pressure coefficient over NACA 0012 airfoil with morphing trailing for Case 1 and Case 5 at angles of attack $\alpha = 0°$ and $4°$ are shown in Fig. 14. The results for Case 1 show a sudden decrease in pressure coefficient on the suction side at $0.7c$ on the flap hinge. The sudden decrease is due to the slight protrusion of the flap hinge into the flow and also due to the impingement of the flow on the flap hinge, where the flow is forced on a sharp turn by the deflection

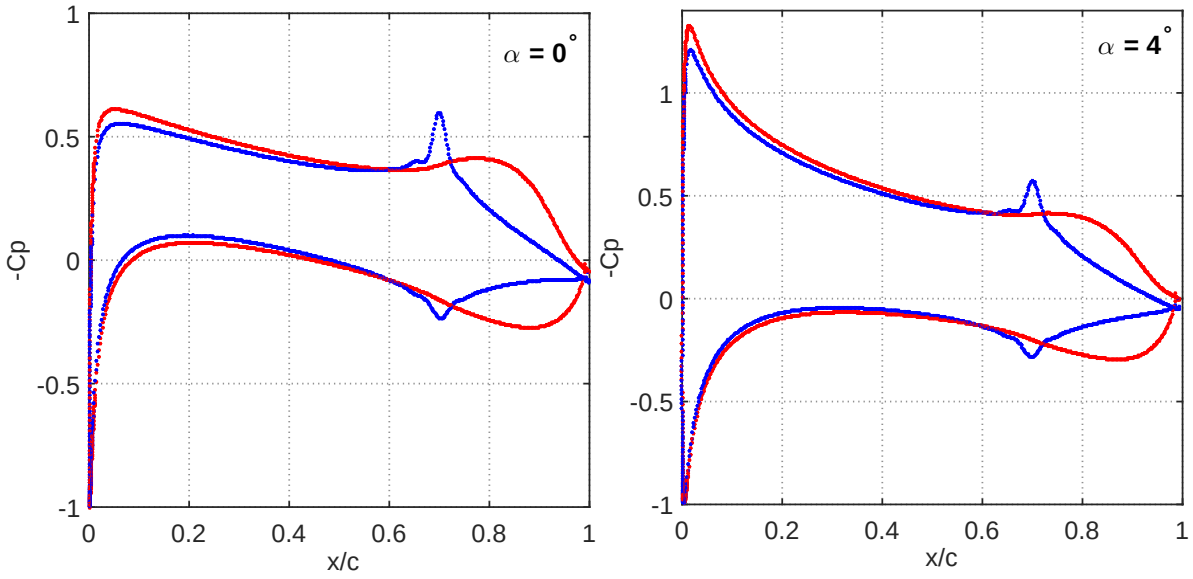

Figure 14. Pressure coefficient distribution over NACA 0012 airfoil with morphing trailing for Case 1 — and Case 5 — at angles of attack $\alpha = 0°$ and $4°$ for flow velocity of $U = 20$ m/s ($Re_c = 2.6 \times 10^5$).

of the trailing edge (flap). From the results it can be observed that Case 5 shows a much well distributed increase in pressure coefficient over the morphing trailing edge ($0.7c$ to $1c$) compared to Case 1. The pressure coefficient increase on the pressure side for Case 5 is much higher than that of Case 1. For Case 5 suction peak has increased by 9% at $\alpha = 0°$ and 8% at $\alpha = 4°$ compared to Case 1, this increase in suction peak can be pointed to the increased velocity at downstream locations over the morphing trailing edge.

IV. Conclusion

Experimental investigation using NACA 0012 airfoil fitted with morphing trailing edges having various camber profiles was carried out to study their effect on the global aerodynamic performance of the airfoil. The airfoil was manufactured using polyurethane working board and CNC machining. The airfoil had a chord and span of $c = 0.2$ m and $l = 0.45$ m, respectively, with a trailing edge deflection angle of $\beta = 5°$ and $10°$. Aerodynamic force measurements, steady and unsteady flow field measurements using hot-wire and several steady state RANS computations using S-A model has been successfully carried out over a wide range of angles of attack ($\alpha = -5°$ to $20°$) and chord-base Reynolds numbers. The lift and drag forces were found to be affected significantly due to the variation in morphing trailing edge profiles. The results showed an increase of up to 13% in $C_{L,max}$ for the highly cambered trailing edge case. However, the drag also increased with increase in the trailing edge camber profile. The L/D ratio at stall angle of attack was reduced only by 4% for the highly cambered trailing edge. Further analysis of the flow velocity at the airfoil downstream wake from hot-wire measurements and computations showed that highly cambered case had larger flow deflection angle and slightly higher velocity deficit. This flow behaviour corresponds to the separation and recirculation observed on the pressure side of the highly cambered case. The results also showed favourable delayed separation on the suction side of the highly cambered case, however the highly cambered case possessed an unfavourable early separation on the pressure side that was absent in the simple hinge flap case. In order to achieve optimum aerodynamic performance with high L/D ratios and delayed flow separation on both the suction and pressure side, the camber of the upper and lower surfaces of the airfoil would have to be morphed independent of each other. Further experimental and computational studies have to be performed for larger trailing edge deflection angles with independent surface morphing trailing edges.

Acknowledgments

This work was supported by the Engineering and Physical Sciences Research Council through the EPSRC Centre for Doctoral Training in Advanced Composites for Innovation and Science [grant number EP/G036772/1]. QA would like to acknowledge the China Scholarship Council for partially funding his study at the University of Bristol.

References

[1] Advisory Council for Aviation Research ans Innovation in Europe, *Strategic Research and Innovation Agenda Executive Summary*, online, http://www.acare4europe.com/sria/exec-summary/volume-1, [accessed on May 08, 2015].

[2] Sinapius, M., Monner, H.P., Kintscher, M., Riemenschneider, J. "DLR's Morphing Wing Activities within the European Network", *Procedia IUTAM*, Vol, 10, pp:416-426, 2014.

[3] Campanile L.F. *Adaptive Structures: Engineering Applications* (Wagg D, Bond IP, Weaver PM, Friswell MI, eds). Wiley:Chichester, 2007. Chapter 4: Lightweight Shape-adaptable Airfoils: A New Challenge for an Old Dream.

[4] Weisshaar, T. "Morphing Aircraft Systems: Historical Perspectives and Future Challenges", *Journal of Aircraft*, Vol.50, NO. 2, pp:337- 353, March 2013. DOI: 10.2514/1.C031456.

[5] Barbarino, S., Bilgen, O., Aja, R.M., Frishwell, M.I., Inman, D.J. "A Review of Morphing Aircraft", *Journal of Intelligent Material Systems and Structures*, Vol. 22, NO. 9, pp:823-877, June 2011. DOI: 10.1177/1045389X11414084.

[6] Chopra, I. "Review of State of Art of Smart Structures and Integrated Systems", *AIAA Journal*,Vol. 40, pp:2145-2187, November 2002. DOI: 10.2514/2.1561.

[7] Lachenal, X., Daynes, S., Weaver, P. " Review of Morphing Concepts and Materials for Wind Turbine Blade Applications",. *Wind Energy*, Vol.16, pp:283-307, March 2013. DOI: 10.1002/we.531.

[8] Daynes, S., Weaver, P.M. "Review of Shape-morphing Automobile Structures: Concepts and Outlooks", *Proceedings of the Institution of Mechanical Engineers, Part D: Journal of Automobile Engineering* , Vol. 227, No. 11, pp:1603-1622, November 2013. DOI: 10.1177/0954407013496557.

[9] Sanders, B., Eastep, F.F., Froster, E. "Aerodynamic and Aeroelastic Characteristics of Wings with Conformal Control Surfaces for Morphing Aircraft", *Journal of Aircraft*, Vol. 40, NO. 1, pp: 94-99, January 2003. DOI: 10.2514/2.3062.

[10] Daynes, S., Weaver, M.P., "A Morphing Trailing Edge Device for a Wind Turbine", *Journal of Intelligent Material Systems and Structures*, Vol. 23, No. 6, pp: 691-701, March 2012. DOI: 10.1177/1045389X12438622.

[11] Thuwis, G.A.A., Abdalla, M.M., Gurdal, Z. "Optimization of a Variable-stiffness Skin for Morphing High-lift Devices", *Smart Materials and Structures*, Vol. 19, No. 12, pp: 124010(10pp), November 2010. DOI:10.1088/0964-1726/19/12/124010.

[12] Wolff, T., Ernst, B., Seume, J.R., "Aerodynamic Behaviour of an Airfoil with Morphing Trailing Edge for Wind Turbine Application", *The Science of Making Torque from Wind 2014 (TORQUE 2014)*, June 2014. DOI:10.1088/1742-6596/524/1/012018.

[13] Campanile, L.F., Anders, S., "Aerodynamic and Aeroelastic Amplification in Adaptive Belt-rib Airfoils", *Aerospace Science and Technology*, Vol. 9, pp:55-63, September 2004. doi:10.1016/j.ast.2004.07.007.

[14] Ai, Q., Azarpeyvand, M., Lachenal, X., Weaver, P., "Aerodynamic and Aeroacoustic Performance of Airfoils Using Morphing Structures , *Wind Energy*, First published online: 16 September 2015, DOI: 10.1002/we.1900.

[15] Ai, Q., Azarpeyvand, M., Lachenal, X., Weaver, P., "Airfoil Noise Reduction Using Morphing Trailing Edge, *The 21st International Congress on Sound and Vibration*, pp. 18, Beijing, China., 13-17, July, 2014.

[16] Yokozeki, T., Sugiura,A., Hirano,Y. "Development of Variable Camber Morphing Airfoil Using Corrugated Structure", *Journal of Aircraft*, Vol. 51, NO. 3, PP:1023-1029, May 2014. DOI: 10.2514/1.C032573.